Chaotic Vibration of the Wave Equation by Nonlinear Feedback Boundary Control

Goong Chen[1], Sze-Bi Hsu[2] and Jianxin Zhou[1]

[1]Department of Mathematics
Texas A&M University, College Station, TX, 77843-3368.
Supported in part by NSF Grant 96-10076 and NATO Grant CRG 940369.
[2]Department of Mathematics
National Tsing Hua University, Hsinchu, Taiwan, Rep. of China.
Supported in part by a grant from the National Council of Science of Rep. of China.

Abstract

Spatiotemporal chaos or turbulence in partial differential equations is a vastly open research field. In this paper, we show that imbalance of boundary energy flow due to certain types of nonlinear feedback boundary control can cause chaotic vibration of the one-dimensional wave equation. We first show that if there is a linear amplifier with feedback gain η at the left end point, and if there is cubic velocity feedback damping at the right end point, then spatiotemporal chaos of the gradient (w_x, w_t) will occur as the gain parameter η is tuned. We then show through numerical simulations of concrete examples what may happen if a more general polynomial feedback is applied at the right end point. Chaotic profiles of wave motion are illustrated by computer graphics.

1.1 Introduction

Advances in dynamical systems, particularly in the theory of chaos, are widely regarded as one of the foremost scientific achievements of the late 20th century. During the past ten years, control theorists have attempted to incorporate brand new techniques in that area in order to understand and utilize nonlinearities in systems. A particularly remarkable new development is *anti-control* – how to create, maintain or enhance chaos when it is healthy and useful [7, p. 4]. Examples of such include fluid mixing, chemical reactions, the biological systems of human brain, heart and perceptual processes, secure communications ([7]), etc. So far, great success has been achieved in the study of *lumped* parameter systems; see [8], for example.

For *distributed* parameter systems, remarkable progress has been made during the past three decades in the *boundary* controllability and stabilizability of linear partial differential equations due to the pioneering work of Russell [17]. Boundary feedback control achieves the control effect on the system by propagating the controller action from the boundary into the interior of the domain. This is quite advantageous from the practical design point of view, because the boundary is much more accessible than the interior of the domain. (Obviously, internally distributed actuators and sensors are also feasible and have already been in use, but their fabrication is more difficult.) A large assortment of highly advanced modern mathematical methods and tools was developed ([1], [14], [15]) to handle the mathematical intricacies. Even though control theorists have also made certain success in treating nonlinear distributed parameter systems, much of the existing work becomes inadequate when the nonlinearity in the system is "severe" with a chaotic regime. Such "genuinely nonlinear" distributed parameter systems display the behavior/phenomena/properties such as multiple unstable solutions, bifurcations, fractals, hysteresis, strange attractors and randomness which can only be approached by the contemporary study in dynamical systems and chaos.

Researchers began to examine chaotic behavior in distributed parameter vibration systems in [13], [18], for example. In [13], Holmes and Marsden derived a Smale horseshoe from the motion of a nonlinear beam. In [18], Sharkovsky considered some chaotic motion of hyperbolic equations. However, no feedback control was mentioned in those works. The efforts made by this group of authors is to study the chaotic behavior of the one-dimensional (1D) linear wave equation when nonlinear feedback is applied at a boundary point. The propagation of acoustic waves in a pipe, and the vibration of a string or a rod, satisfy the linear wave equation

$$w_{xx}(x,t) - w_{tt}(x,t) = 0, \qquad 0 < x < L, t > 0, \tag{1.1.1}$$

where the subscripts xx of w_{xx}, e.g., denote twice partial differentiations with respect to the x variable. Let the initial conditions (ICs) be

$$w(x,0) = w_0(x), \quad w_t(x,0) = w_1(x), \qquad 0 < x < L. \tag{1.1.2}$$

Let the boundary conditions (BCs) be, respectively,

$$w_t(0,t) = -\eta w_x(0,t), \qquad t > 0, \tag{1.1.3}$$

$$w_x(L,t) = \alpha w_t(L,t) - \beta w_t^3(L,t), \qquad t > 0, \tag{1.1.4}$$

at the left end $x = 0$ and the right end $x = L$, where α, β and η are positive constants lying in certain parameter ranges. The BC (1.1.4) is associated with the name of van der Pol in that it has the effect of self-regulation or self-excitation [19] and is therefore extremely useful in the design of servomechanisms in automatic control. The cubic nonlinear relation in (1.1.4) can be realized by using tunnel diodes ([2, Appendix C]), for example. The left BC (1.1.3) is linear signifying the presence of an *amplifier* (such as a microphone in acoustics); it injects energy into the system,where the *energy* of wave motion at time t is defined by

$$E(t) = \frac{1}{2}\int_0^L [w_x^2(x,t) + w_t^2(x,t)]dx. \tag{1.1.5}$$

Note that the parameter η in (1.1.3) may be considered as the *feedback gain*; this gain will be the varying parameter in most of discussions to follow. The above statements will be clear if we look at the rate of change of energy of the system:

$$\begin{aligned}\frac{d}{dt}E(t) &= \int_0^L [w_{xt}w_x + w_{tt}w_t]dx \\ &= \cdots \text{(integration by parts and utilization of (1.1.3) and (1.1.4))} \\ &= \eta w_x^2(0,t) + w_t^2(L,t)[\alpha - \beta w_t^2(L,t)],\end{aligned} \tag{1.1.6}$$

where

(i) $\eta w_x^2(0,t) \geq 0$, meaning that energy is injected into the system from the left endpoint;

(ii)
$$w_t^2(L,t)[\alpha - \beta w_t^2(L,t)] \begin{cases} \geq 0, & \text{if } |w_t(L,t)| \leq (\alpha/\beta)^{1/2}, \\ < 0, & \text{if } |w_t(L,t)| > (\alpha/\beta)^{1/2}. \end{cases}$$
signifying a self-regulation effect.

The *imbalance of boundary energy flow* is evident in (1.1.6), as we see that the effect of the left end BC is trying to increase the total energy of the system, while that of the right end BC is to modulate the total energy

change. In [3], [4], we have shown that when α, β and η enter a certain regime, chaotic vibration of the gradient (w_x, w_t) occurs. Note that in (1.1.3), *force feedback* (i.e., the $-\eta w_x(0,t)$ term) is used, while in (1.1.4), *nonlinear velocity feedback* (i.e., $\alpha w_t(L,t) - \beta w_t^3(L,t)$ terms) is used. Also, we mention that in [3, (93)] (which is a differentiated form of (1.1.4)) a combination of *nonlinear displacement and velocity feedback* is used.

In this paper, we consider chaotic vibrations generated by *polynomial velocity feedback* at the right end boundary point. The organization of the paper is as follows:

(1) In §II, we prove that when the van der Pol BC (1.1.4) is replaced by one with *cubic damping*, chaotic vibration still happens when the parameters enter a certain range. This shows that imbalance of boundary energy flow is a major cause of chaos, and the nonlinearity does not have to be van der Pol in order for chaos to occur.

(2) In §III, we show through numerical simulations certain new features of nonlinear phenomena when higher order polynomial velocity feedback is used at the right endpoint.

The study in (1) and (2) above leads to many pertinent questions whose detailed treatment must be deferred to a sequel where more space is available.

1.2 Chaos Induced by Interaction of Energy Injection at the Left End and Cubic Damping at the Right End

Let us clearly state the problem under consideration:

$$w_{xx}(x,t) - w_{tt}(x,t) = 0, \qquad 0 < x < 1, t > 0, \tag{1.2.1}$$

$$w_t(0,t) = -\eta w_x(0,t), \qquad t > 0; \eta > 0, \eta \neq 1, \tag{1.2.2}$$

$$w_x(1,t) = -[\alpha w_t(1,t) + \beta w_t^3(1,t)], \qquad t > 0; \alpha \geq 0, \beta > 0, \tag{1.2.3}$$

$$w(x,0) = w_0(x), \quad w_t(x,0) = w_1(x), \qquad 0 < x < 1. \tag{1.2.4}$$

Comparing (1.2.3) with (1.1.4), we note that the α here has been given a different sign so that the RHS of (1.2.3) now represents a cubic damping velocity feedback (without the van der Pol self-regulation effect). We also mention that we have set L in (1.1.2) to be 1, because the velocity of wave propagation can be easily incorporated and adjusted in the ensuing analysis. The standard change of variables ([2]-[4])

$$w_x = u + v, \quad w_t = u - v \tag{1.2.5}$$

converts (1.2.1)-(1.2.4) to a diagonalized first order hyperbolic system

$$\frac{\partial}{\partial t}\begin{bmatrix} u \\ v \end{bmatrix} = \begin{bmatrix} 1 & 0 \\ 0 & -1 \end{bmatrix} \frac{\partial}{\partial x}\begin{bmatrix} u \\ v \end{bmatrix}, \tag{1.2.6}$$

$$v(0,t) = G_\eta(u(0,t)) \equiv \frac{1+\eta}{1-\eta}u(0,t), \tag{1.2.7}$$

$$u(1,t) = F_{\alpha,\beta}(v(1,t)) \equiv v(1,t) + g_{\alpha,\beta}(v(1,t)), \tag{1.2.8}$$

$$u(x,0) \equiv u_0(x) = \frac{1}{2}[w_0'(x) + w_1(x)], \quad 0 < x < 1,$$

$$v(x,0) \equiv v_0(x) = \frac{1}{2}[w_0'(x) - w_1'(x)], \ 0 < x < 1, \tag{1.2.9}$$

where in (1.2.8), the nonlinear function $g_{\alpha,\beta}(v)$ is defined implicitly through the cubic equation

$$\beta g_{\alpha,\beta}^3(v) + (1+\alpha)g_{\alpha,\beta}(v) + 2v = 0, \tag{1.2.10}$$

and $F_{\alpha,\beta}(v) \equiv v + g_{\alpha,\beta}(v)$. By an application of the Implicit Function Theorem and a little extra effort, it is easy to show that $g_{\alpha,\beta}(v)$ is a globally well-defined (single-valued) function. By the tracing of characteristics ([2, 10]), the unique solution to (1.2.6)-(1.2.9) can be given explicitly below: For $t = 2k + \tau$, $k = 0, 1, 2, \ldots, 0 \le \tau < 2$ and $0 \le x \le 1$,

$$u(x,t) = \begin{cases} (F_{\alpha,\beta} \circ G_\eta)^k(u_0(x+\tau)), & \tau \le 1-x, \\ G_\eta^{-1} \circ (G_\eta \circ F_{\alpha,\beta})^{k+1}(v_0(2-x-\tau)), & 1-x < \tau \le 2-x, \\ (F_{\alpha,\beta} \circ G_\eta)^{k+1}(u_0(\tau+x-2)), & 2-x < \tau \le 2; \end{cases} \tag{1.2.11}$$

$$v(x,t) = \begin{cases} (G_\eta \circ F_{\alpha,\beta})^k(v_0(x-\tau)), & \tau \le x, \\ G_\eta \circ (F_{\alpha,\beta} \circ G_\eta)^k(u_0(\tau-x)), & x < \tau \le 1+x, \\ (G_\eta \circ F_{\alpha,\beta})^{k+1}(v_0(2+x-\tau)), & 1+x < \tau \le 2. \end{cases} \tag{1.2.12}$$

Here, as a rather standard practice in dynamical systems, we have abused the notation $(F_{\alpha,\beta} \circ G_\eta)^k$, e.g., to denote the kth iterate composition of the function $F_{\alpha,\beta} \circ G_\eta$ with itself. *Spatiotemporal chaotic vibration* of u and v occurs when the map $F_{\alpha,\beta} \circ G_\eta$ and/or $G_\eta \circ F_{\alpha,\beta}$ is/are chaotic. Representations (1.2.11) and (1.2.12) show that u and v are completely determined by the composite reflection relations $G_\eta \circ F_{\alpha,\beta}$, $F_{\alpha,\beta} \circ G_\eta$, and their iterates. But $F_{\alpha,\beta} \circ G_\eta$ and $G_\eta \circ F_{\alpha,\beta}$ are topologically conjugate to each other [3, p. 433], so it is sufficient to consider whether $G_\eta \circ F_{\alpha,\beta}$ alone is chaotic. The map $G_\eta \circ F_{\alpha,\beta}$ is thus a natural *Poincaré section* of the PDE system (1.2.1)-(1.2.4) or (1.2.5)-(1.2.6).

For easy visualization, we display the graphs of $G_\eta \circ F_{\alpha,\beta}$ for certain sample values of α, β and η in Fig. 1.

(a)

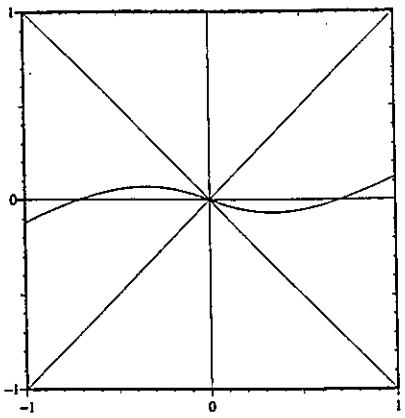

(b)

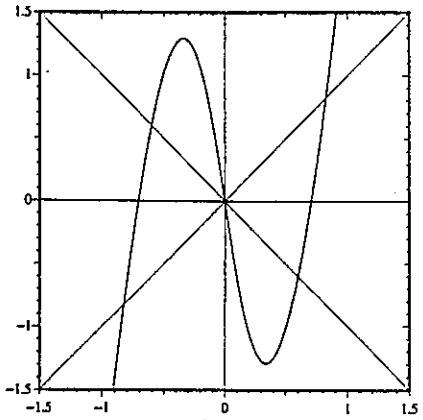

(c)

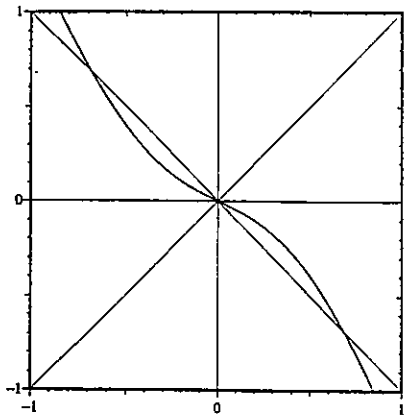

FIGURE 1
Graphs of the map $G_\eta \circ F_{\alpha,\beta}$: (a) $\eta = 0$, $\alpha = 0.5$, $\beta = 1$; (b) $\eta = 0.9$, $\alpha = 0.5$, $\beta = 1$; (c) $\eta = 1.5$, $\alpha = 1.2$, $\beta = 1$.

LEMMA 1.1 Stability of the Origin
Let $\alpha \geq 0$ and $\beta > 0$. Then

(i) If $\alpha = 0$, then the origin is a neutrally stable fixed point and is (weakly) globally attracting.

(ii) If $\alpha > 0$, then the origin is a globally attracting fixed point of $F_{\alpha,\beta}$.

(iii) If $0 < \alpha < 1$ and either $1 > \eta > \alpha$ or $\eta > 1$, then the origin is a repelling fixed point of $G_\eta \circ F_{\alpha,\beta}$.

(iv) If $\alpha > 1$ and either $0 < \eta < 1$, $\alpha\eta > 1$ or $\alpha > \eta > 1$ then the origin is a repelling fixed point of $G_\eta \circ F_{\alpha\beta}$.

PROOF By differentiating the function $g_{\alpha,\beta}$ in (1.2.10) implicitly, it is easy to obtain

$$F'_{\alpha,\beta}(v) = 1 + g'_{\alpha,\beta}(v) = 1 - \frac{2}{3\beta g^2_{\alpha,\beta}(v) + (1+\alpha)}. \tag{1.2.13}$$

At $v = 0, g_{\alpha,\beta}(0) = 0$, so we obtain

$$F'_{\alpha,\beta}(0) = 1 - \frac{2}{1-\alpha} = \frac{\alpha - 1}{\alpha + 1}; \quad |F'_{\alpha,\beta}(0)| \leq 1 \text{ for } \alpha \geq 0. \tag{1.2.14}$$

Conclusions in (i) and (ii) above become immediately clear from (1.2.13) and (1.2.14).

Since

$$(G_\eta \circ F_{\alpha,\beta})'(0) = \frac{1+\eta}{1-\eta} \cdot \frac{\alpha - 1}{\alpha + 1}, \tag{1.2.15}$$

we easily verify the claims in (iii) and (iv). □

LEMMA 1.2 v-axis Intercepts
Let $\alpha \geq 0$, $\beta > 0$, $\eta > 0$ and $\eta \neq 1$ be given. Then for $0 \leq \alpha < 1$, the map $G_\eta \circ F_{\alpha,\beta}$ has three distinct v-axis intercepts

$$v = -\sqrt{\frac{1-\alpha}{\beta}}, 0, \sqrt{\frac{1-\alpha}{\beta}}. \tag{1.2.16}$$

For $\alpha \geq 1$, $G_\eta \circ F_{\alpha,\beta}$ has exactly one intercept at $v = 0$.

PROOF Obvious from [3, Lemma 2.3]. □

THEOREM 1.3
(Period-Doubling Bifurcation Theorem for $-G_\eta \circ F_{\alpha,\beta}, 0 < \eta < 1$)
Let $\alpha \geq 0$ and $\beta > 0$ be fixed, and let η: $\eta > \alpha$, be a varying parameter such that $1 - \alpha\eta > 0$. Then

(i) $v_0(\eta) \equiv \frac{1+\eta}{2}\sqrt{\frac{\eta-\alpha}{\beta}}$ *is a curve of fixed points of* $-G_\eta \circ F_{\alpha,\beta}$*:*

$$-G_\eta \circ F_{\alpha,\beta}(v_0(\eta)) = v_0(\eta). \tag{1.2.17}$$

(ii) The algebraic equation

$$\frac{1}{2}\left(\frac{1-\alpha\eta}{3\beta\eta}\right)^{1/2}\left[\frac{1+(3+2\alpha)\eta}{3\eta}\right] = \frac{1+\eta}{2}\sqrt{\frac{\eta-\alpha}{\beta}} \tag{1.2.18}$$

has a unique solution $\eta = \eta_0$ *for any given* α*:* $0 \le \alpha \le 1$ *and* $\beta > 0$*. We have*

$$\frac{\partial}{\partial v}[-G_\eta \circ F_{\alpha,\beta}(v)]|_{\substack{v=v_0(\eta_0)\\ \eta=\eta_0}} = -1. \tag{1.2.19}$$

(iii) For $\eta = \eta_0$ *satisfying (1.2.18), we have*

$$\begin{aligned} A &\equiv -\left[\frac{\partial^2(G_\eta \circ F_{\alpha,\beta})}{\partial\eta\partial v} - \frac{1}{2}\left(\frac{\partial}{\partial\eta}G_\eta \circ F_{\alpha,\beta}\right)\frac{\partial^2}{\partial v^2}(G_\eta \circ F_{\alpha,\beta})\right]\Bigg|_{\substack{v=v_0(\eta_0)\\ \eta=\eta_0}} \\ &= -\frac{[4\alpha(2\alpha-3)+6]\eta_0^3 + (6-4\alpha)\eta_0^2 - 10\eta_0 + 6}{3(1-\eta_0)^3(1+\eta_0)^2} \\ &\neq 0. \end{aligned} \tag{1.2.20}$$

(iv) For η_0 *given in (ii), we have*

$$\begin{aligned} B &\equiv -\left[\frac{1}{6}\frac{\partial^3(G_\eta \circ F_{\alpha,\beta})}{\partial v^3} - \frac{1}{4}\left(\frac{\partial^2(G_\eta \circ F_{\alpha,\beta}))^2}{\partial v^2}\right)^2\right]\Bigg|_{\substack{v=v_0(\eta_0)\\ \eta=\eta_0}} \\ &= \frac{8\beta\eta_0^4\{(1-\eta_0)[5-(1+6\alpha)] + 6\eta_0(1+\alpha\eta_0)\}}{(1-\eta_0)^2(1+\eta_0)^4} > 0. \end{aligned} \tag{1.2.21}$$

Consequently, there is period-doubling bifurcation at $(v_0(\eta_0), \eta_0)$*. The stability type of the bifurcated period-2 orbit is attracting.*

PROOF The assertions in (i)-(iv) above are adaptations of [3, Theorem 3.1] by changing α therein to $-\alpha$. The only restrictions we must observe are that $\eta > \alpha \ge 0$ and $1 - \alpha\eta > 0$. It is straightforward to verify (i). We can also confirm (ii)-(iv) with computer-aided proofs. Therefore the Period-Doubling Bifurcation Theorem [16, pp. 220-223] applies. □

Example 1.1
By setting $\alpha = 0.5$ and $\beta = 1$ in (1.2.19) and solve for $\eta = \eta_0$ on the computer, we obtain

$$\eta_0 \approx 0.7676. \tag{1.2.22}$$

This value at which the first period-doubling occurs can be observed in Fig. 2. □

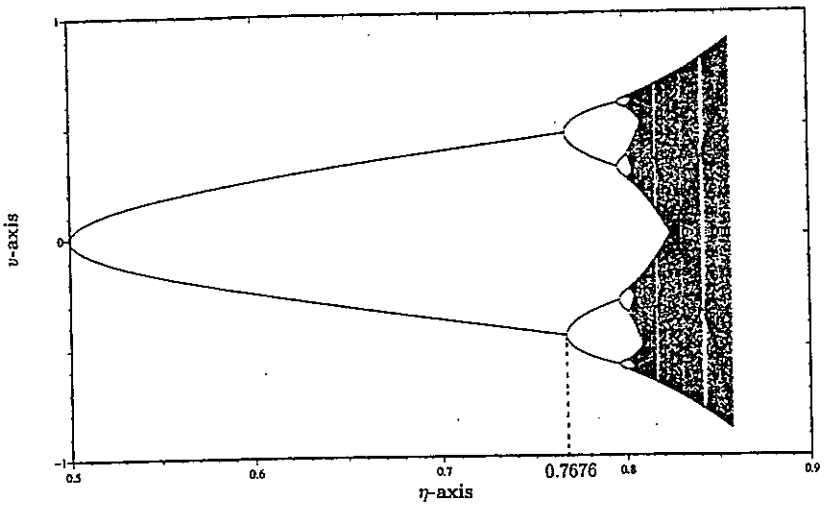

FIGURE 2
The orbit diagram of the map $G_\eta \circ F_{\alpha,\beta}$, where we have chosen fixed $\alpha = 0.5$, $\beta = 1$, and let η vary in [0,1). Note that the first period-doubling bifurcation happens at $\eta_0 \approx 0.7676$, agreeing with (1.2.22).

A period-doubling bifurcation may or may not lead to a *full period-doubling cascade* and the consequent chaos, depending on whether the map $-G_\eta \circ F_{\alpha,\beta}$ has the renormalizable property [9], [12]. Here we note that every prime period-2^n orbit of the map $-G_\eta \circ F_{\alpha,\beta}$ corresponds to a unique prime period-2^{n+1} orbit of the map $G_\eta \circ F_{\alpha,\beta}$ [3, Lemma 3.1]. The map $-G_\eta \circ F_{\alpha,\beta}$ is *unimodal* on $[0,\infty)$ and $(-\infty,0]$, respectively. Therefore, renormalizability is assured. However, the restrictions $\eta > \alpha \geq 0$ and $1 - \alpha\eta > 0$ must also be satisfied all the time. Numerical simulations have indicated that under these restrictions, a full period-doubling cascade will always follow. This is supported by Theorem 2 below, where the existence of homoclinic orbits is shown, which is a surefire way to establish chaos [11, Theorem 1.16.5].

THEOREM 1.4
(Homoclinic Orbits and Homoclinic Bifurcations of the Map $G_\eta \circ F_{\alpha,\beta}$ for $0 \leq \alpha < 1$ with respect to the Varying Parameter η: $0 < \eta < 1$) *Let $0 \leq \alpha < 1, \beta > 0$, and define*

$$\underline{\eta}_H = \underline{\eta}_H(\alpha) = \left(1 - \frac{1-\alpha}{3\sqrt{3}}\right) \Big/ \left(1 + \frac{1-\alpha}{3\sqrt{3}}\right).$$

If η satisfies $1 > \eta \geq \underline{\eta}_H$, then 0 is a repelling fixed point of the map $G_\eta \circ F_{\alpha,\beta}$ having homoclinic orbits. Furthermore, if $\eta = \underline{\eta}_H$, then there are degenerate homoclinic orbits.

Consequently, if $\eta \in [\underline{\eta}_H, 1)$, then the map $G_\eta \circ F_{\alpha,\beta}$ is chaotic on some invariant sets of $G_\eta \circ F_{\alpha,\beta}$.

PROOF It is easy to check that if $1 > \eta \geq \underline{\eta}_H$, then

$$1 > \eta \geq \left(1 - \frac{1-\alpha}{3\sqrt{3}}\right) \Big/ \left(1 + \frac{1-\alpha}{3\sqrt{3}}\right) > \alpha,$$

and therefore $\frac{1+\eta}{1-\eta} \cdot \frac{\alpha-1}{\alpha+1} > 1$ the origin becomes a repelling fixed point by (1.2.15) and Lemma 1.1 (iii).

The rest follows easily from an adaptation of [3, Theorem 4.1] by setting α to $-\alpha$ therein. Since the arguments are identical, we refer the reader to [3, loc. cit.]. □

Contrary to [3, Theorem 4.2], the origin of the map $G_\eta \circ F_{\alpha,\beta}$ does not have homoclinic orbits when $\eta > 1$. This is also partly evident from Fig. 1(c).

The chaotic property of the family of maps $G_\eta \circ F_{\alpha,\beta}$ with α and β fixed and varying η is evident from the orbit diagram in Fig. 2, where $\alpha = 0.5$ and $\beta = 1$ are chosen.

If we break up the overall reflection map $G_\eta \circ F_{\alpha,\beta}$, we have

(i) G_η is a linear expansion map;

(ii) $F_{\alpha,\beta}$ is a nonlinear contraction map.

The interactions of linear expansion and nonlinear contraction can lead to chaos. This is the major conclusion of this section. What can be said about a contrasting case, a composite map $\widetilde{G}_\eta \circ \widetilde{F}_{\alpha,\beta}$, where

(i)′ $\widetilde{G}_\eta$ is a linear contraction map;

(ii)″ $\widetilde{F}_{\alpha,\beta}$ is a nonlinear expansion map?

We can achieve (i)′ by changing BC (1.2.2) to

$$w_t(0,t) = \eta w_x(0,t), \quad \eta > 0,$$

leading to

$$\widetilde{G}_\eta(u) \equiv \frac{1-\eta}{1+\eta} u,$$

and achieve (ii)′ by changing BC (1.2.3) to

$$w_x(0,t) = \alpha w_t(0,t) + \beta w_t^3(0,t), \qquad \alpha, \beta > 0, \alpha \geq 1,$$

yielding

$$\widetilde{F}_{\alpha,\beta}(v) = v + g_{\alpha,\beta}(v),$$

where $g_{\alpha,\beta}(v)$ is (uniquely defined as) the solution of

$$\beta g^3_{\alpha,\beta}(v) + (\alpha - 1)g_{\alpha,\beta}(v) - 2v = 0, \qquad v \in \mathbb{R}.$$

Our numerical simulations so far have indicated that the map $\widetilde{G}_\eta \circ \widetilde{F}_{\alpha.\beta}$ is never chaotic throughout the entire parameter range $\eta > 0$, $\alpha \geq 1$ and $\beta > 0$. This seems to be in sharp contrast to the chaos-causing potential of the map $G_\eta \circ F_{\alpha,\beta}$ in the theorems and graphics in this section.

1.3 Feedback of Polynomial Type at the Right Endpoint

The preceding section has shown that the nonlinear feedback does not have to be of the van der Pol type in order for chaotic vibration to occur. This has set the tone in this section for exploring a larger class of nonlinear feedback boundary controls at the right endpoint, which, after interaction with energy injection at the left endpoint, lead to chaos.

The broadest class of nonlinear boundary conditions at the right endpoint can be described by an implicit nonlinear equation

$$\mathcal{F}(w(1,t), w_x(1,t), w_t(1,t)) = 0, \qquad t > 0,$$

involving all the boundary displacement ($w(1,t)$), force ($w_x(1,t)$) and velocity ($w_t(1,t)$) variables. But this class is too general to be useful for control purposes. At this point, it is not clear to the authors what would be "the most natual" choice for $\mathcal{F}$ based upon the physical consideration, either. Two choices, much narrower but mathematically quite reasonable, would be

(1) a polynomial feedback of velocity to the force, in the form

$$w_x(1,t) = P_n(w_t(1,t)), \tag{1.3.1}$$

where $P_n(\cdot)$ is a polynomial of degree n given by

$$P_n(z) = a_n z^n + a_{n-1} z^{n-1} + \cdots + a_2 z^2 + a_1 z,$$

or

(2) a polynomial feedback of force to the velocity, in the form

$$w_t(1,t) = P_n(w_x(1,t)). \tag{1.3.2}$$

Note that we have not permitted the presence of the displacement variable $w(1,t)$ in either (1.3.1) or (1.3.2) since the corresponding mathematical treatment would be substantially more involved and, so far, few results are available even for very simple $P_n's$.

From purely the mathematical point of view, equations (1.3.1) and (1.3.2) can be handled in the same fashion. For definiteness, let us just study type (1.3.1) throughout the rest of the paper. As before, using (1.2.5) in (1.3.1) and write out in detail:

$$u + v = \sum_{k=1}^{n} a_k (u - v)^k, \qquad (u = u(1,t), v = v(1,t))$$

we obtain

$$u = F_a(v) \equiv v + g_a(v), \tag{1.3.3}$$

where $g_a(v)$ is defined implicitly through the nonlinear equation

$$\sum_{k=2}^{n} a_k g_a^k(v) + (a_1 - 1) g_a(v) - 2v = 0, \qquad v \in \mathbb{R}. \tag{1.3.4}$$

For each given $v \in \mathbb{R}$, (1.3.4) may have as many as n real solutions $g_a(v)$ and, thus, in general, $g_a(v)$ is not a well-defined function of v. (In reality, multivalued $g_a(v)$ is *physically admissible.* What one has is a *hysteresis* situation. Certain special cases have been treated in [4], for example. For general multivalued functions $g_a(v)$, however, the hysteresis behavior will be quite complicated. No systematic study has been done so far.) To avoid this technical difficulty, it is sufficient to assume that

$$P_n'(x) - 1 = \sum_{k=2}^{n} k a_k x^{k-1} + (a_1 - 1) \neq 0, \qquad \forall\, x \in \mathbb{R}. \tag{1.3.5}$$

Under (1.3.5), we have either $P_n'(x) - 1 > 0$ or $P_n'(x) - 1 < 0$ for all $x \in \mathbb{R}$, the Implicit Function Theorem then applies and (with a few extra arguments) we have the single-valuedness of the function $g_a(v)$.

At this point of time, there is no theory available about the dynamic behavior of the composite reflection map $G_\eta \circ F_a$, where G_η and F_a are defined, respectively, in (1.2.7) and (1.3.3). We envision that the development of such a theory will be a major task for us in the next few years. Nevertheless, in what follows we do wish to present two concrete examples to illustrate the novel dynamic features and, perhaps, the advantages of using polynomial feedback boundary control in generating chaotic vibration of the wave equation.

Example 1.2

Assume (1.2.1)-(1.2.4), except that the right end BC (1.2.3) is replaced by

$$w_x(1,t) = -w_t^5(1,t) + 4w_t^4(1,t) - 6w_t^3(1,t) + 0.5w_t(1,t), \quad t > 0. \quad (1.3.6)$$

It is easy to check that here

$$\begin{aligned} P_5'(x) - 1 &= -5x^4 + 16x^3 - 18x^2 - 0.5 \\ &= -x^4 - 4x^2(x-2)^2 - 2x^2 - 0.5 < 0, \qquad \forall\, x \in \mathbb{R}, \end{aligned}$$

and, therefore, we have a well-defined function $F_a(\cdot)$; its graph is displayed in Fig. 3. A distinctive feature observed from Fig. 3 is that F_a is not unimodal, nor is it an odd function (in contrast to those counterparts studied in [2]-[6]).

We now study the asymptotic dynamic behavior of the composite reflection map $G_\eta \circ F_a$ by varying $\eta \in \mathbb{R}, \eta \neq 1$. The orbit diagram is plotted in Fig. 4.

From this orbit diagram, we observe the following features:

(a) For larger values of η (i.e., η away from 1), the orbits of $G_\eta \circ F_a$ consist essentially of two branches, with each branch functioning at its own will, for positive v and negative v, separately. For example, the upper branch has already completed the period-doubling cascade (when η decreases leftward toward 1) and is well into chaos, while the lower branch is still undergoing its first period-doubling bifurcation.

(ii) For η in the approximate range [1.751, 1.877], the chaos in the upper branch is suddenly sucked out of existence by attracting periodic orbits of the lower branch, causing "disconnectedness" or "gap" between the two branches.

(iii) The two branches re-attach for $\eta \in (1.488, 1.751)$.

(iv) Another chaotic regime exists for $\eta < 0.633$.

To show some of the chaotic effects of the above spatiotemporally, let us choose $\eta = 1.9417$, with the following ICs:

$$\begin{cases} v_0(x) = 10(x - \frac{1}{2}) \cdot \phi_0(x), & x \in [0,1], \\ u_0(x) \equiv 0, & x \in [0,1], \end{cases} \quad (1.3.7)$$

where $\phi_0(x)$ is a C^2-continuous piecewise cubic spline defined by

$$\phi_0(x) = \frac{1}{24} \begin{cases} (x - x_1)^3/h^3, & x_1 \le x \le x_2, \\ 1 + \dfrac{3(x-x_2)}{h} + \dfrac{3(x-x_2)^2}{h^2} - \dfrac{3(x-x_2)^3}{h^3}, & x_2 \le x \le x_3, \\ 1 - \dfrac{3(x-x_4)}{h} + \dfrac{3(x-x_4)^3}{h^2} + \dfrac{3(x-x_4)^3}{h^3}, & x_3 \le x \le x_4, \\ (x_5 - x)^3/h^3, & x_4 \le x \le x_5, \\ 0, & \text{elsewhere}, \end{cases}$$

$$h = 1/6, x_j = j/6, \qquad j = 1, 2, 3, 4, 5.$$

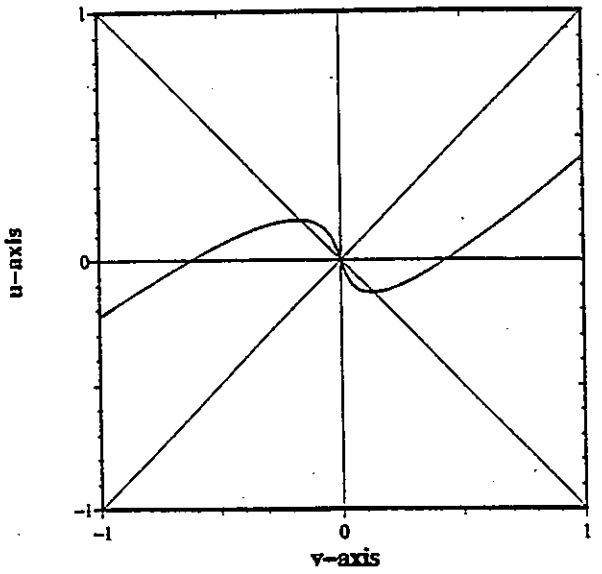

FIGURE 3
Graph of the map F_a in Example 1.2.

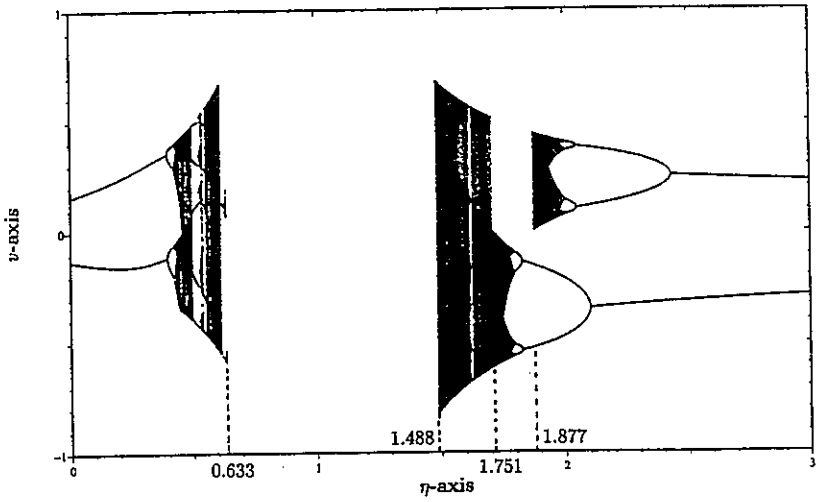

FIGURE 4
The orbit diagram of the map $G_\eta \circ F_a$ with η varying in $(0, 3)$.

The choice in (1.3.7) implies the corresponding choice of the ICs for w, the original state variable in (1.2.1), to be

$$\begin{cases} w_0(x) = w(x,0) = \displaystyle\int_0^x w_x(\xi,0)d\xi + C \\ \qquad\qquad\quad = \displaystyle\int_0^x v_0(\xi)d\xi + C, C = \text{ arbitrary constant}, \\ w_1(x) = w_t(x,0) = u_0(x) - v_0(x) = -v_0(x). \end{cases}$$

According to [3, Theorem 6.1], we have the regularities

$$(u,v) \in [C^2([0,1]\times[0,T])]^2,$$

$$(w,w_t) \in C^3([0,1]\times[0,T]) \times C^2([0,1]\times[0,T]), \text{ for any } T>0.$$

The initial spatiotemporal profiles of (u,v) and (w_x,w_t) are plotted, respectively, in Figs. 5 and 6, for $(x,t) \in [0,1]\times[0,2]$.

In this example, each *cycle of vibration*, defined to be the time duration required for a wave to travel from $x=0$ to $x=1$, reflect at $x=1$ and return to $x=0$, is two time units. So let us look at the snapshots of (u,v) during the 50th time cycle, $t = 101.5 \in [50\cdot 2, 51\cdot 2] = [100,102]$, displayed in Figs. 7(a) and (b). We observe that u and v manifest both chaotic and periodic behavior. This can be easily interpreted with the visual aid of Fig. 8.

It is known that (w_x,w_t) and (u,v) are topologically conjugate in the sense of [6, §IV]. The profile of w is not displayed here. It has a *fractal* look but does *not* display chaotic behavior; cf. [6, Fig. 6.11], for example. In order to make w itself chaotic, the nonlinear BC must contain w; see [3, Theorem 6.2]. □

Example 1.3

Let us return to (1.2.1)-(1.2.4) again, but with (1.2.3) replaced by

$$w_x = -\frac{1}{\mu}(\frac{1}{5}w_t^5 - w_t^4 - \frac{1}{3}w_t^3 + 8w_t^2) - \left(1 - \frac{12}{\mu}\right)w_t; \qquad (\mu = 12.6618) \tag{1.3.8}$$

at $x=1$, for all $t>0$. Then we have

$$\begin{aligned} P_5'(x) - 1 &= -\frac{1}{\mu}(x^4 - 4x^3 - x^2 + 16x - 12) - 2 \\ &= -\frac{1}{\mu}[(x+1)(x+2)(x+3)(x-2)] - 2 \\ &= -\frac{|m|}{\mu}\left\{\frac{1}{|m|}[(x+1)(x+2)(x+3)(x-2)]\right\} - 2 \\ &< \frac{|m|}{\mu} - 2 < 0, \quad \forall x \in \mathbb{R}, \end{aligned} \tag{1.3.9}$$

(a)

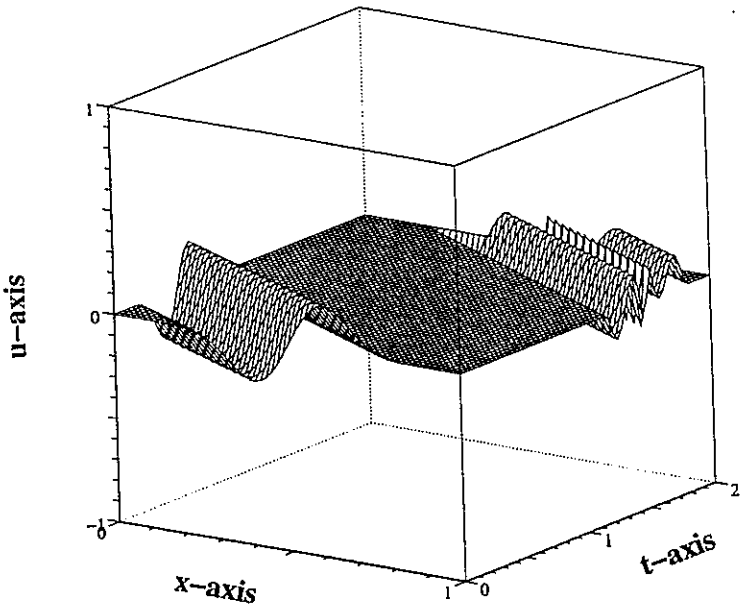

(b)

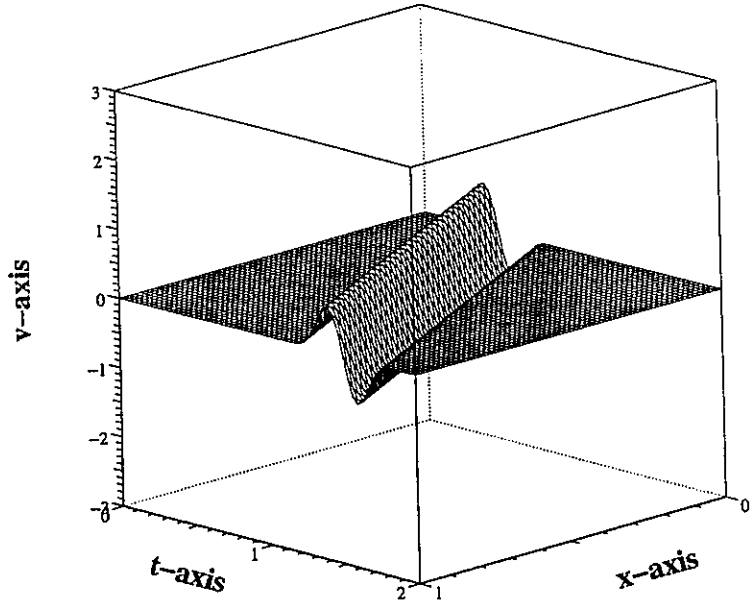

FIGURE 5
The initial spatiotemporal profiles of: (a) u and (b) v, for $x \in [0,1]$ and $t \in [0,2]$ in Examples 1.2.

(a)

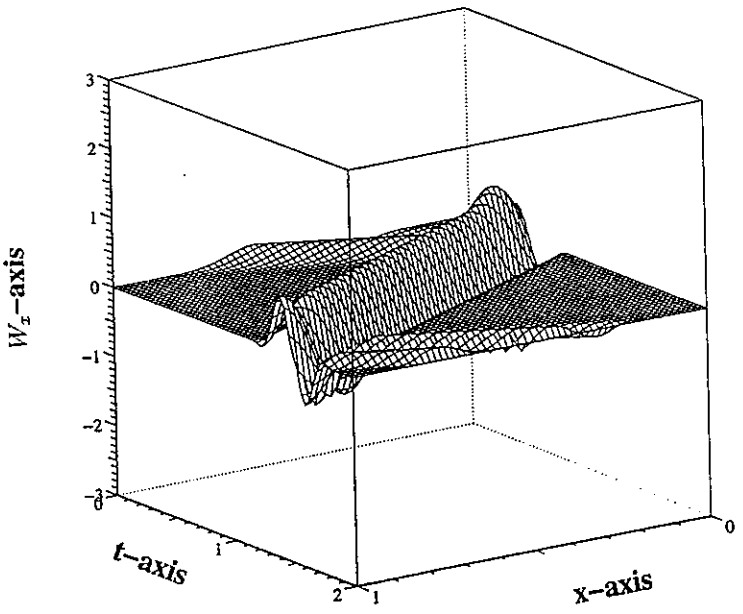

(b)

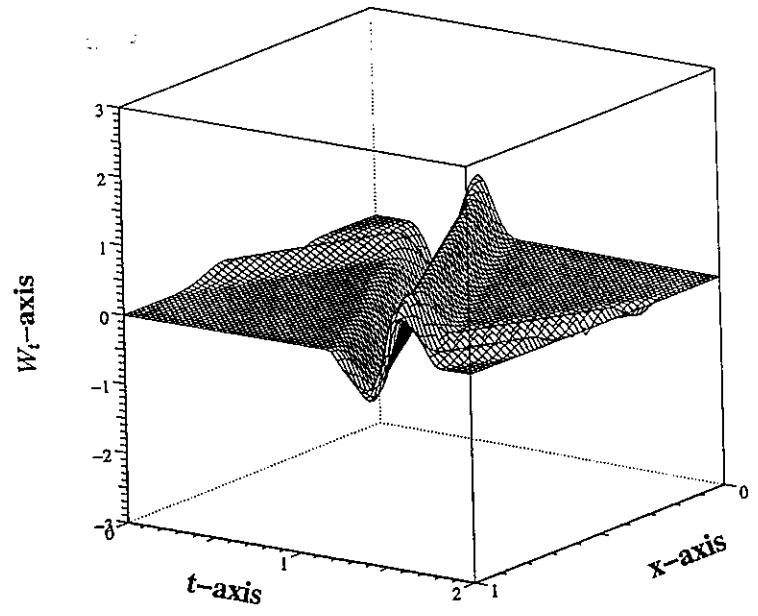

FIGURE 6
The initial spatiotemporal profiles of: (a) w_x and (b) w_t, for $x \in [0,1]$ and $t \in [0,2]$ in Example 1.2.

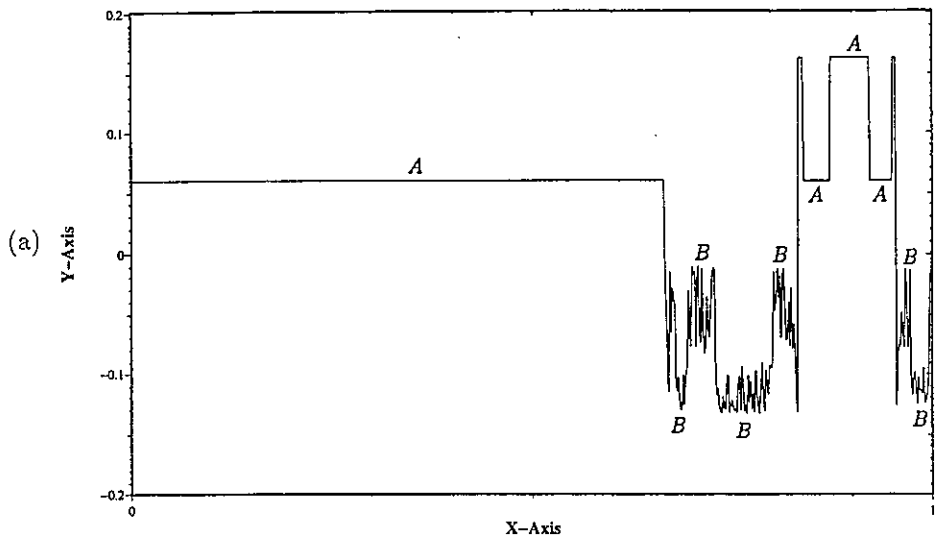

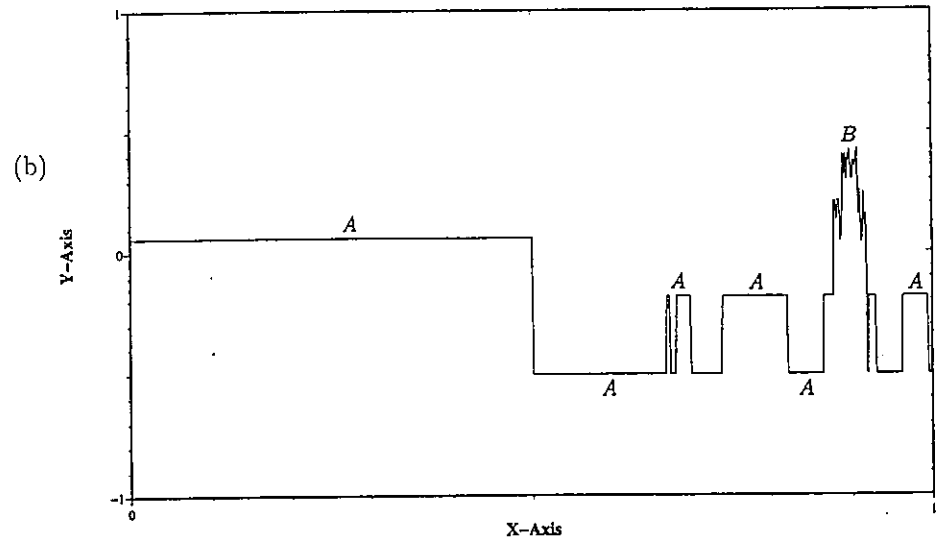

FIGURE 7
The snapshots of: (a) u and (b) v, for $x \in [0,1]$ and $t = 101.5 \in [100, 102]$ in Example 1.2. Note that the "flat parts" indicated by A correspond to the periodic portion of the solution, while the "highly oscillatory parts" indicated by B correspond to the chaotic portion of the solution. Thus u and v have mixed behavior of being partly periodic and partly chaotic.

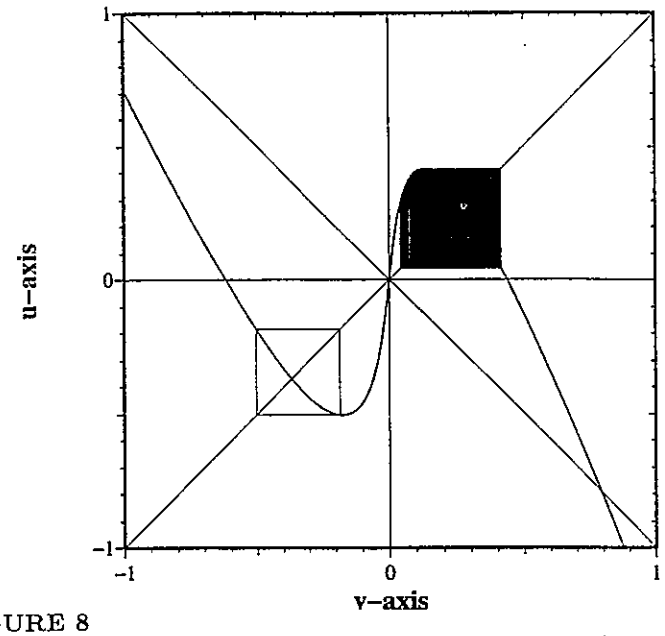

FIGURE 8
This graphical analysis shows coexistence of chaos (for $v > 0$) and attracting period-2 orbits (for $v < 0$) of the map $G_\eta \circ F_{\alpha,\beta}$, with $\eta = 1.9417$, for Example 1.2. Note that for $v > 0$, the iterates of $G_\eta \circ F_{\alpha,\beta}$ are chaotic as shown by the denseness of orbits in the middle upper right of the figure, while for $v < 0$ the iterates converge to a period-2 orbit in the middle lower left of of the figure.

where

$$m = \inf_{x \in \mathbb{R}} [(x+1)(x+2)(x+3)(x-2)] \approx -24.0572$$

and by the choice of μ we have $\frac{|m|}{\mu} < 2$ and, therefore (1.3.5) is satisfied. The reflection map F_a at the right endpoint is well-defined, which is computed and then shown in Fig. 9. Comparing it with the counterpart F_a for Example 1.2 in Fig. 3, we see that Fig. 9 embodies more features – it has two local maxima and two local minima. (These four local extremal points are somehow "designed" to be related to the four roots of the polynomial $(x+1)(x+2)(x+3)(x-2)$ in (1.3.9).)

The orbit diagram of $G_\eta \circ F_a$ is shown in Fig. 10 for the varying parameter $\eta < 1$. Here again we see chaos. For η appearing in some range, it is straightforward to *rigorously establish* that the origin is a repelling fixed point *having homoclinic orbits*, and hence chaos ensues. See Proposition 1 below. But how about other causes/routes to chaos? The initial period doubling route to chaos seems to have disappeared. Can we still characterize the onset of chaos without period-doubling?

The "irregular" pattern of the orbit diagram in Fig. 10 leaves many questions waiting to be answered. □

The proof of the following proposition, although stated in a form applicable only to Example 3 above, contains ideas which can be used to treat general problems.

PROPOSITION 1.5
Let F_a be the map (1.3.3) defined through the boundary feedback relation (1.3.8) in Example 3. Then for η lying in a certain range of the interval $(0,1)$, the origin is an unstable fixed point having homoclinic orbits for the map $G_\eta \circ F_a$.

PROOF Since homoclinic orbits are geometric concept and their existence can be confirmed "visually", an "intuitive proof" suffices provided that all the geometric conditions are met.

First, we observe from Fig. 9 that the origin (as a fixed point of $G_0 \circ F_a = F_a$) does not have homoclinic orbits. However, as η increases from 0, $\frac{1+\eta}{1-\eta} \cdot m$ begins to decrease past I_ℓ (cf. the caption of Fig. 9 for the values of m and I_ℓ), and at the same time the origin becomes a repelling fixed point.

A homoclinic orbit is marked by dotted lines in Fig. 11, where we have chosen $\eta = 0.45$. □

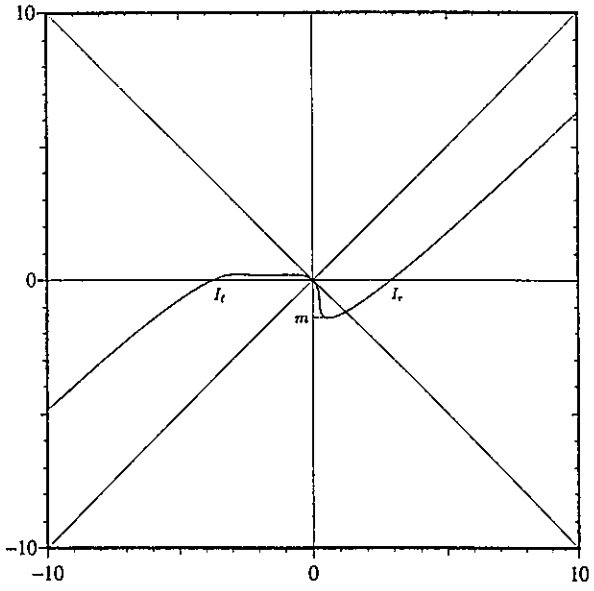

FIGURE 9
The graph of the reflection map F_a at $x = 1$ in Example 1.3. In addition to the origin, there are two intercepts as indicated: $I_r \approx 2.8846$ and $I_\ell \approx -3.7260$. A local minimum value $m \approx -1.4321$ is also marked.

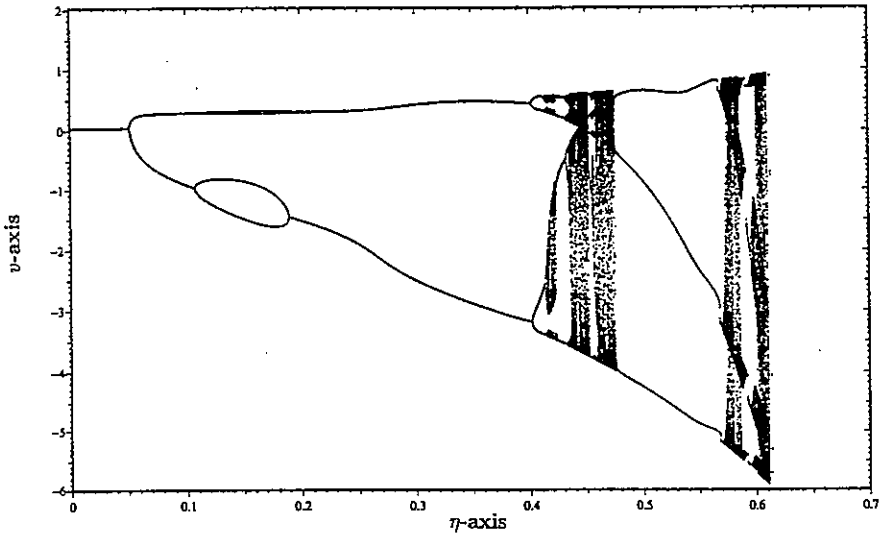

FIGURE 10
The orbit diagram of $G_\eta \circ F_a$ with the varying parameter $0 < \eta < 1$ for Example 1.3.

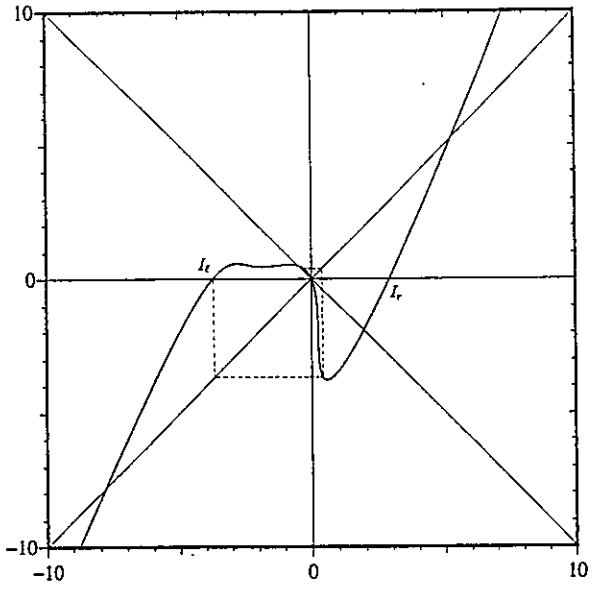

FIGURE 11
The dotted lines indicate a homoclinic orbit for the map $G_\eta \circ F_a$ in Example 3 and Proposition 1, where $\eta = 0.45$ is chosen.

1.4 Concluding Remarks

Only the one-dimensional wave equation is treatable so far by the types of nonlinear feedback control (or anti-control) in this chapter. For "similar" equations arising in structural vibration such as the Euler-Bernoulli beam equation, although some reflection relations on the boundary may be defined, the work here cannot be extended to that case when the boundary condition is nonlinear because the wave propagation on an Euler-Bernoulli beam is *dispersive*.

In higher dimensional settings, the study of partial differential equations with nonlinear boundary conditions is a rather difficult subject in itself, let alone that of chaotic effects caused by nonlinear boundary feedback. At present, the best hope seems to be offered by problems on domains with special geometry such as the rectangular, spherical and annular cases.

In any case, the advent of modern dynamical systems and chaos has provided the control theorist with many useful ideas and powerful tools to explore as well as to exploit nonlinearities in distributed parameter control systems, with bright, aplenty future opportunities in this field.

[17] D. L. Russell, "Controllability and stabilizability theory for linear partial differential equations, recent progress and open questions," *SIAM Review*, Vol. 20 pp. 383-431, 1978.

[18] A. N. Sharkovsky, "Ideal turbulences in an idealized time-delayed Chua's circuit," *Int. J. Bifurcation & Chaos*, Vol. 4 pp. 303-309, 1994.

[19] J. J. Stoker, *Nonlinear Vibrations*, Wiley-Interscience, New York, 1950.